Instant Determination of Earth's Polar Motion by Lunar Laser Ranging Common View

Zhipeng LIANG[1,2], Chengzhi LIU[1,3], Jinsong PING[2,4], Makram Ibrahim[5],

[1] Changchun Observatory of National Astronomical Observatories, Chinese Academy of Sciences, Changchun, 130117, China; *lcz@cho.ac.cn*

[2] University of Chinese Academy of Sciences, Beijing, 101408, China

[3] Key Laboratory of Space object and Debris Observation, Purple Mountain Observatory, Chinese Academy of Sciences, Nanjing, 210008, China

[4] National Astronomical Observatories, Chinese Academy of Sciences, Beijing, 100101, China

[5] National Research Institute of Astronomy and Geophysics, Helwan, 11421, Cairo, Egypt

Abstract The Lunar Laser Ranging (LLR) technology has been used to determine the Earth Rotation Parameters (ERP) since the 1970s. Conventional determination methods incorporate state-of-the-art models and LLR data spread over decades. The up-to-date studies achieve an accuracy of tens of microseconds for UT1 and several milliarcseconds (mas) for polar motion coordinates (PMC). This paper determines the instant PMC using the lunar laser ranging common view method (LLRCV). Through quantitative analysis of derivatives of lunar range residual to ERP variation, we formulated a linear equation to solve for the instant PMC with simultaneous range measurements. The precision of the solution were evaluated from the precision of the measurement through the analysis of the linear equation. We found 184 LLRCV events in the LLR data during 2012-2022 to solve for PMC. To form the solution errors, the results of our method are compared to the IERS C04 data. The results showed that 29.3% of the solution errors were less than 150 mas, and 21.7% of the solutions were more accurate than the prediction data. This method has the potential to address short-term and transient geophysical changes. Nonetheless, its dependence on long-term geodetic data means it is not a substitute for conventional techniques.

Key words: reference systems — Moon — methods: data analysis — planets and satellites: general

1 INTRODUCTION

The Lunar Laser Ranging (LLR) is the measurement of round-trip time between a ground laser ranging station (station) and a lunar retro-reflector array (reflector). Over the past decade, several LLR observation stations have produced precise data. These stations are located in Grasse of France (GRSM), Wettzell of Germany (WETL), and Matera of Italy (MATM) in Europe, as well as Apache Point (APOL) and McDonald Observatory (MDOL) of the United States of America in North America (Murphy 2013; Chabé et al. 2019). The precision of LLR measurement has improved to centimeter level (Samain et al. 1998; Chabé et al. 2019). In recent years, two laser ranging stations in China reported acquisition of LLR data (Huang et al. 2022; Yan & Guo 2024) .

LLR data has been used to determine components of the Earth rotation parameter (ERP) since the 1970s (Bender et al. 1973; Müller et al. 2019). Typical early research determined UT0 and variation of latitude from one night of lunar ranging data, to achieve an accuracy of 0.7 milliseconds or 10 milliarcseconds (mas) (Stolz et al. 1976). Modern LLR data analysis, which incorporate up-to-date reference frame data and state-of-the-art models about all aspects of the Earth and moon, is able to determine all components of ERP (Hofmann et al. 2018; Müller et al. 2019; Pavlov 2020; Singh et al. 2022). Typical modern research on ERP determination selects observation nights with 10-15 normal points (Hofmann et al. 2018; Pavlov 2020; Singh et al. 2022). Most up-to-date studies achieve the accuracy of several mas for polar motion coordinates (PMC) (Hofmann et al. 2018; Singh et al. 2022).

The ERP components fitted in the traditional way represent the long-term evolution of Earth rotation, rather than the real-time status of Earth rotation. Major geodynamic events, such as earthquakes, can cause rapid changes in Earth's rotation parameters (Xu & Sun 2012; Xu et al. 2014). Therefore, it is of interest to determine instant ERP components, to provide data for time-sensitive geodetic studies.

The concept of lunar laser ranging common view (LLRCV) dates back to as early as the 1980s (Leick 1980). Leick proposed the concepts of simutaneous observation from pairs of co-observing stations, and investigated the determination of ERP components, with simulated lunar laser range differencing data (Leick 1980). It was claimed that the method could provide ERP components with measurement accuracy on Earth's surface, which was about 30 cm for LLR in the early 1980s (Leick 1980). This accuracy corresponds to 10 mas for PMC, or 0.6 ms for UT1 (Leick 1980).

Another form of lunar range common view was proposed by Müller et al., to place an optical transponder on the lunar surface to illuminate the whole facing hemisphere of Earth, thus enabling common-view ranging at standard SLR stations, to yield 1000 times improvement of detected photons than tranditional LLR (Müller et al. 2009).

The challenge in the common view approach is the bad geometry. Given a single session of LLRCV measurements, it is not possible to determine all three ERP components at that epoch. This is because LLR range measurements are invariant to the rotation about the axis from the Earth's center to the reflector. As a result, the rotation angle cannot be determined by LLR data. The LLRCV method can only determine two independent linear combinations of the three ERP components. And if the reflector is near the equator plane, polar motion components become unsolvable.

To overcome the rank deficiency, more measurements are needed, at different lunar hour angles, as suggested in early studies (Leick 1980; Dickey et al. 1985). However, taking more measurements at multiple epochs involves the dynamics of both the Earth and the moon, which may introduce complexities in modeling. This paper focuses on instant determination with simultaneous common-view measurements in a single epoch.

In this paper, we succeeded in determining PMC using LLRCV data sessions, with each session acquired simultaneously from a pair of stations. The method of determination with LLRCV is presented in Section 2, where the LLR measurement model and ERP variation model are formulated in common view scenarios, and the scheme for instant determination and assessment is described. In Section 3, we introduce the measurement data and ERP data used in this paper. The results are shown and discussed in Section 4. A discussion is given in Section 5.

2 INSTANT ERP DETERMINATION

The model for lunar laser ranging has been presented by numerous works (Chapront & Francou 2006; Müller et al. 2009; Murphy 2013; Hofmann et al. 2018; Müller et al. 2019; Pavlov 2020).

The lunar ranging measurement conducted from a ground station to a lunar reflector can be modeled as:

$$\tau = s_{12}/c + s_{23}/c + \tau_{\mathrm{gr}} + \tau_{\mathrm{tropo}} + \Delta\tau$$

, where τ represents the time of flight measured in the station, the distances s_{12} and s_{23} represent the vacuum light path from station to reflector (outbound) and reflector to station (inbound), respectively, accounted in barycentric inertial coordinates. The relativistic delay τ_{gr} represents the gravitational delay effect on the flying pulse. The tropospheric delay τ_{tropo} represents the tropospheric refraction delay during light propagation. Correction term $\Delta\tau$ is accounted for the difference between TT and TDB clock rates.

These terms are quantified using either Terrestrial Time (TT), Barycentric Dynamical Time (TDB), or International Atomic Time (TAI). The round-trip time interval τ is meant to be measured in Earth observatory with an atomic time scale, TAI. Laser flight paths s_{12} and s_{23} are calculated with TDB-compatible barycentric ephemeris, therefore the corresponding time of flight are calculated in TDB. The general relativity correction τ_{gr} is calculated in TDB, too. The tropospheric delay τ_{tropo} is modeled in TT. The correction term $\Delta\tau$ is calculated in TT. During the lunar ranging round trip time, less than 3 seconds, $\Delta\tau$ is 10^{-12} second level, which is negligible in this paper.

Light paths s_{12} and s_{23} are the Euclidean distances. The s_{12} is from the station at transmit time t_1 to the reflector at hit time t_2, and s_{23} is from the reflector at t_2 to the station at receive time t_3, as following:

$$s_{12} = |\vec{s_{12}}| = |-\vec{r_{\mathrm{ES}}}(t_1) - \vec{r_{\mathrm{BE}}}(t_1) + \vec{r_{\mathrm{BM}}}(t_2) + \vec{r_{\mathrm{MA}}}(t_2)|$$

$$s_{23} = |\vec{s_{23}}| = |-\vec{r_{\mathrm{MA}}}(t_2) - \vec{r_{\mathrm{BM}}}(t_2) + \vec{r_{\mathrm{BE}}}(t_3) + \vec{r_{\mathrm{ES}}}(t_3)|$$

, where $\vec{r_{\mathrm{ES}}}$, $\vec{r_{\mathrm{BE}}}$, $\vec{r_{\mathrm{BM}}}$, $\vec{r_{\mathrm{MA}}}$ are barycentric vectors with B for barycenter of the solar system , E for the Earth center, S for the ground station, M for moon center, and A for retro-reflector array, respectively. The barycentric vectors $\vec{r_{\mathrm{BE}}}$ and $\vec{r_{\mathrm{BM}}}$ are computed with the TDB-compatible DE430 planetary ephemeris. The selenocentric vector $\vec{r_{\mathrm{MA}}}$ is computed with selenocentric coordinates and lunar libration angles, both

provided by DE430 ephemeris (Folkner et al. 2014; Williams et al. 2013). The geocentric station vector $\vec{r_{ES}}$ is calculated using the ITRF2020 coordinates and transformed into a geocentric celestial reference frame.

Algorithms for reference system conversion between celestial and terrestrial frames, terrestrial tide off-sets, tropospheric refraction delay of light propagation, relativistic delay of light propagation in gravitation field, and relativistic motion deformation of Earth and moon, are adopted from IERS conventions 2010 (Petit 2010; Luzum & Petit 2012).

Time scale conversion algorithms are adopted from SOFA (Hohenkerk 2012), especially the PyMsOfa software package (Ji et al. 2023). Other astronomical calculations are conducted with AstroPy (Price-Whelan et al. 2022).

Comparing the LLR model against historical LLR data from year 2012 to 2022, we get range residuals, as shown in Subsection 3.3.

2.1 Determination of Earth rotation parameters with LLRCV

The Earth rotation parameters (ERP) represent Euler angles of Earth rotation in the geocentric celestial reference system (GCRS). Conventionally, the Earth rotation parameter (ERP) contains one set of three numbers. The rotation axis is represented by terrestrial intermediate pole (TIP) coordinates, or polar motion coordinates (PMC), noted as x_p, y_p. The Earth rotation angle (ERA) ψ_{ERA} in the celestial reference frame, concerning the equinox, is represented by UT1. The conversion formula between ERA (mod 2π) and UT1 (mod 24h) is $\psi_{ERA} = 15 \times 1.00273781191135448 \times$ UT1, with UT1 in second and ERA in arc-second. The three ERP components y_p, x_p, and ψ_{ERA} are related to frame rotations about the X, Y, and Z axes, respectively.

We assume the vector of ERP variation solely causes the variation of LLR measurement, i.e., $\delta\rho = \frac{\partial\rho}{\partial y_p}\delta y_p + \frac{\partial\rho}{\partial x_p}\delta x_p + \frac{\partial\rho}{\partial\psi_{ERA}}\delta\psi_{ERA}$. At a given epoch, we assume that two or more stations (A,B,...) simultaneously conducted range measurements, to form range residual vector $\vec{q} = (\delta\rho_A, \delta\rho_B, ...)^T$. Then we form linear equation $M\vec{p} = \vec{q}$, where the design matrix M holds partial derivatives of range measurements to ERP components. The calculation of design matrix M involves only predicted ERP data. About the predicted ERP data, see Subsection 3.1.

In this paper, we focus on the determination of the polar motion components δx_p and δy_p using two simultaneous measurements from a pair of common view stations. In such a problem, the design matrix M is shaped 2 by 2, and the parameter vector $\vec{p} = (\delta y_p, \delta x_p)^T$. The x_p and y_p predictions were calculated with a linear model as described in Subsection 3.1. The UT1 data are set to reference data. After solving for $\vec{p}$, we adjust the prediction with $\vec{p}$ to form an estimate of x_p and y_p. The estimated ERP components were then compared with the reference data for assessment.

2.2 Variation Analysis of Lunar Range Measurements

To investigate the variation $\delta\rho$ of lunar range measurement ρ to ERP components y_p, x_p, ψ_{ERA}, or partial derivatives, we start with the geometrical relation:

$$\delta\rho = H(\theta, \varphi)\delta\vec{r}_{GCRS} \tag{1}$$

, where $H(\theta, \varphi) = (-\cos\theta\cos\varphi, -\sin\theta\cos\varphi, -\sin\varphi)$ is the transpose of the unit vector along the line of sight from the reflector to the station. Angles θ and φ are celestial right ascension and declination of the reflector, as seen from the station. The variation vector $\delta\vec{r}_{\text{GCRS}}$ is the variation of the station's geocentric inertial vector, caused by ERP variation.

According to the IERS Conventions 2010 (Petit 2010), the transformation from an international terrestrial reference system(ITRS) to a geocentric celestial reference system(GCRS) is:

$$\vec{r}_{\text{GCRS}} = Q(t)R_3(-s')\left(R_3(-\psi_{\text{ERA}})R_2(x_p)R_1(y_p)\right)\vec{r}_{\text{ITRS}}$$

,where the bracketed term $R_3(-\psi_{\text{ERA}})R_2(x_p)R_1(y_p)$ is where the ERPs take effect. The term $Q(t)$ is the transformation matrix arising from the motion of the celestial pole in the celestial reference system, i.e. precession and nutation, and R_1, R_2, R_3 are matrices for coordinate frame rotation about axes X, Y and Z. We adapted the equation to its current form using commutativity between terrestrial intermediate origin (TIO) locator $R_3(-s')$ and the Earth rotation $R_3(-\psi_{\text{ERA}})$.

The variations of astronomical angles θ and φ due to ERP changes are negligible. We apply partial derivative rules on the above equation Equation (1), and let the ERP components be predicted values $(y_p^0, x_p^0, \psi_{\text{ERA}}^0)$, then we have partial derivatives as:

$$\frac{\partial\rho}{\partial p_1} = M_{\text{HQR}}R_3(-\psi_{\text{ERA}}^0)R_2(x_p^0)R_1'(y_p^0)\cdot\vec{r}_{\text{ITRS}}$$

$$\frac{\partial\rho}{\partial p_2} = M_{\text{HQR}}R_3(-\psi_{\text{ERA}}^0)R_2'(x_p^0)R_1(y_p^0)\cdot\vec{r}_{\text{ITRS}}$$

$$\frac{\partial\rho}{\partial p_3} = -M_{\text{HQR}}R_3'(-\psi_{\text{ERA}}^0)R_2(x_p^0)R_1(y_p^0)\cdot\vec{r}_{\text{ITRS}}$$

, where $M_{\text{HQR}} = H(\theta, \varphi)Q(t)R_3(-s')$. The matrices $R_k'(k = 1, 2, 3)$ denote the derivatives of each rotation matrix with respect to the rotation angle.

2.3 Precision of Solution

The precision of the solution is used for quality assessment of the solutions, before the comparison with reference data. It mainly depends on the stiffness of the design matrix M .

According to the perturbation theorem of linear algebra, for any linear system $Ax = b$ and its perturbed form $(A + \delta A)(x + \delta x) = b + \delta b$, we have the following inequality (Shores 2018) : $\frac{\|\delta x\|}{\|x\|} \leq \frac{\text{cond}(A)}{(1-c)}\left\{\frac{\|\delta A\|}{\|A\|} + \frac{\|\delta b\|}{\|b\|}\right\}$, where $\text{cond}(A) = \|A\|\|A^{-1}\|$ is the condition number of matrix A, and $c = \|A^{-1}\delta A\|$ should satisfy $c < 1$. The latter requirement means the perturbation should be minor. In this work, we assume the perturbations in the coefficient matrix are relatively small, i.e. $\frac{\|\delta A\|}{\|A\|} \approx 0$. Therefore we neglect c and $\frac{\|\delta A\|}{\|A\|}$, letting them be zero in the formula. The inequality becomes $\frac{\|\delta x\|}{\|x\|} \leq \text{cond}(A)\frac{\|\delta b\|}{\|b\|}$ and then

$$\frac{\|\delta x\|}{\|\delta b\|} \leq \text{cond}(A)\frac{\|x\|}{\|b\|}$$

.

For the problem of the PMC determination, we put the design matrix M, the PMC correction vector $\vec{p}$ and range residual vector $\vec{q}$ into the formula. If we put range measurement precision (NP RMS) vector $\delta\vec{q}$

into the place of δb and move it to the right end, the resulting inequality $\|\delta \vec{p}\| \leq \|\delta \vec{q}\| \cdot \text{cond}(M) \frac{\|\vec{p}\|}{\|\vec{q}\|}$ puts an upper bound on the norm of the solution error $\delta \vec{p}$. We call the upper bound the precision of the solution. It means how much the solution would be perturbed given the measurement precision as variation in the range measurement, and it also represents the resolving power of the instant determination method.

3 DATA

3.1 ERP data

The reference ERP dataset was adopted from the IERS EOP 20 C04 time series, retrieved from the IERS website. (Luzum et al. 2020). The precision of polar motion coordinates in reference data was better than 0.1 mas in the selected time span.

The predicted polar motion data were needed as initial input for the solution. The IERS (2010) mean pole model (Petit 2010) was adopted to calculate predictions. After epoch 2010.0, the model is formulated as: [1]

$$\bar{x}_p(t) = 23.513 + 7.6141 \times (t - t_0)$$

$$\bar{y}_p(t) = 358.891 - 0.6287 \times (t - t_0)$$

, where t and t_0 are Besselian epochs [2] of current time and year 2000, respectively, with $\bar{x}_p$ and $\bar{y}_p$ units in mas. The deviations between prediction and reference are no more than 200 mas for both components in the selected period. See Figure 1.

3.2 Terrestrial and Lunar Coordinates

The coordinates of ground observatories are mostly adopted from the International Terrestrial Reference Frame (ITRF) 2020 (Altamimi et al. 2023). Since the APOL station is not included in ITRF2020, we adopted its coordinates from (Hofmann et al. 2018). Small adjustements to station coordinates are made to optimize LLR range residuals. The adjusted station coordinates are listed below in Table 1.

The reflector coordinates are initially adopted from the DE430 document and adjusted with range residuals, which are listed below in Table 2.

3.3 Lunar Laser Ranging

We retrieved 10513 LLR normal point (NP) data from the EUROLAS Data Center (EDC) [3], with a period from 2012 May 2 to 2022 December 7, provided by stations APOL, GRSM, MATM, MDOL, and WETL, as shown in Figure 2 (a) and (b).

In the LLR data, the Consolidated Ranging Data (CRD) format allows the recording of normal point root mean square (RMS) numbers, which is considered equivalent to 1-sigma. The following Figure 3 shows measurement precision of the existing LLR stations during the years 2012-2022.

---

[1] (IERS (2010) mean pole model TN36(7.25))

[2] Julian epochs are also acceptable by the model.
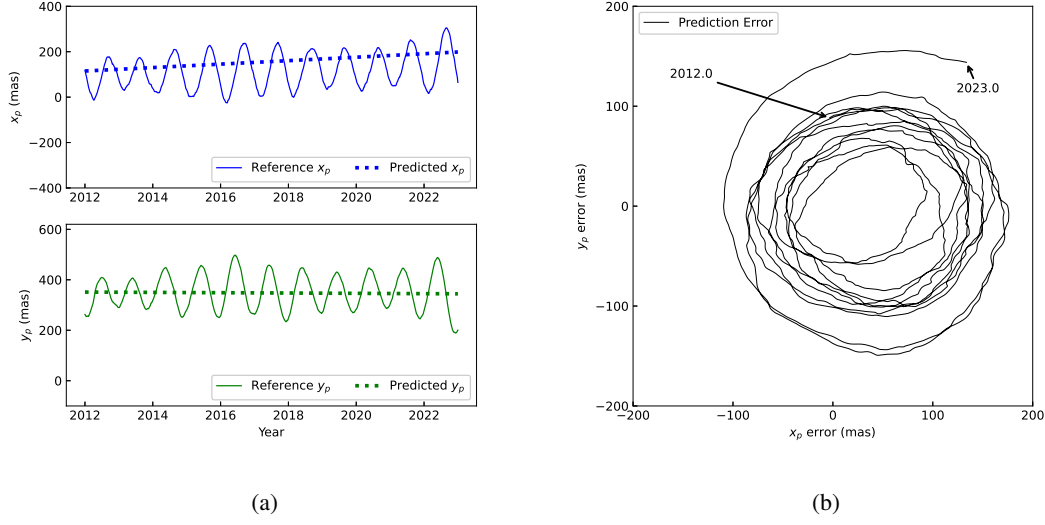
[3] *http://edc.dgfi.tum.de*

(a) (b)

Fig. 1: The prediction, the reference and the prediction error series of polar motion coordinates x_p and y_p during the period from 2010 to 2022. In (a), the predicted (dotted line) and reference (solid curve) time series of x_p (blue) and y_p (green) components are shown. In (b), the prediction error series of pole motion coordinates is shown in two-dimension curve (solid curve). The prediction error of PMC evolves around the origin (0,0) not exceeding ±200 mas.

Table 1: Station coordinates used in this paper

Name /IDNo.	Location	x (m)	y (m)	z (m)	longitude (deg)	latitude (deg)	height (m)
APOL(7045)	Apache Point, USA	-1463999.073	-5166632.621	3435012.802	-105.8204	32.7804	2786.5504
GRSM(7845)	Grasse, France	4581691.775	556196.341	4389355.231	6.9216	43.7546	1323.1842
MATM(7941)	Matera, Italy	4641978.524	1393067.820	4133249.696	16.7046	40.6487	536.9815
MDOL(7080)	McDonald, USA	-1330021.294	-5328401.839	3236474.876	-104.0152	30.6802	2001.3067
WETL(8834)	Wettzell, Germany	4075576.182	931785.739	4801584.126	12.8780	49.1444	665.4118

Notes: The cartesian coordinates are based on the ITRF2020 frame. The longitude, latitude and height data are approximate.

We filtered 0.8% (88 of 10513) outlier NPs of which the range residuals were larger than 0.4 meter. In the adopted 99.2% (10425 of 10513) NP data, the range measurement residuals against the model is 0.05 meters.

3.4 Common View Events

We searched the historical LLR normal point (NP) data for common view events, where two normal points from different stations have a temporal separation of less than one hour. The epoch of a common view event was set to the mid-point of the pair of NP epochs. From the above mentioned LLR data, we found 184 common view events as listed in the Table 3. The GRSM station formed common-view events with MATM for 126 times and with WETL for 55 times. The APOL station formed common view with MDOL for 3 times. Due to geological separation, the stations in Europe did not form common view events with stations

Table 2: Reflector coordinates used in this paper

Name	x	y	z	longitude	latitude	height
	(m)	(m)	(m)	(deg)	(deg)	(m)
apollo11	1591748.076	691220.843	20398.420	23.4730	0.6735	-1927.6
luna17	1114957.971	-780934.909	1075633.109	-35.0080	38.3152	-2471.4
apollo14	1652818.172	-520455.918	-110360.813	-17.4787	-3.6442	-1064.3
apollo15	1554937.340	98603.741	764413.168	3.6285	26.1334	-1923.0
luna21	1339388.601	802309.554	755849.750	30.9221	25.8323	-2761.3

Notes: The cartesian coordinates are based on the moon centered mean Earth frame. The longitude, latitude and height data are approximate.
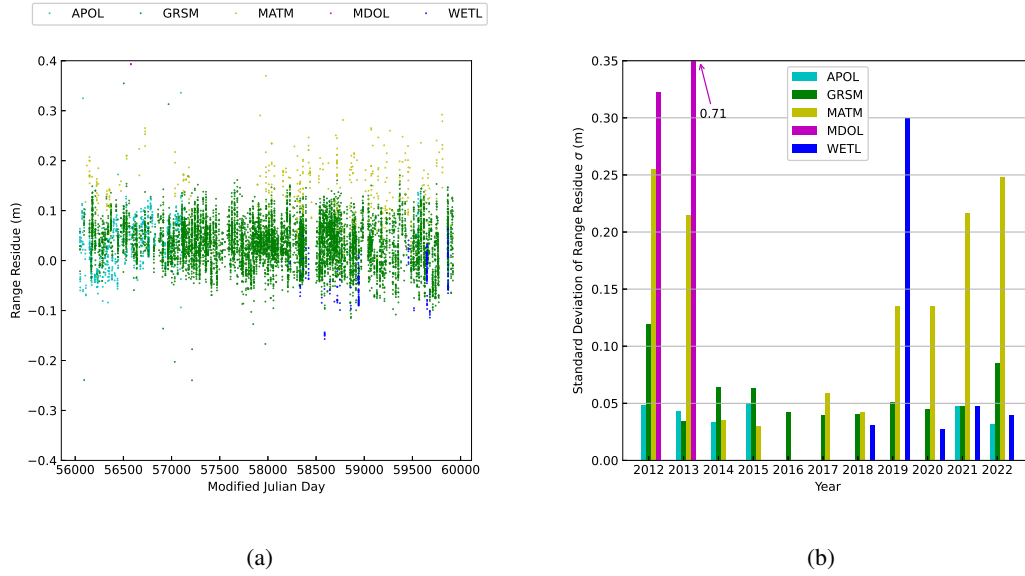
Fig. 2: LLR range residuals from 2012 to 2022. In (a), each dots represents the range residual of a normal point compared against the LLR model. In (b), bars represent the standard deviation of the range residuals in each year. The points and bars are colored by station.

in America. Out of all common-view events, the reflector Apollo-15 was the most frequently tracked, with a total of 119 events. The other reflectors tracked included 30 events from Luna-17, 17 events from Apollo-11, 13 events from Luna-21, and 5 events from Apollo-14.

The common view events are dense during certain times when the lunar phase and weather were suitable for LLR observation by adjacent stations.

4 DATA ANALYSIS

For each common view event, we solved the corresponding polar motion components x_p and y_p. The solution represents the instant value of the mentioned parameters at the epoch of the common view event. We analyzed the precision and accuracy of the solutions.

Comparing the polar motion solution with reference polar motion data, the solution errors were generated. By fitting solution error versus solution precision, we found an empirical uncertainty trend curve
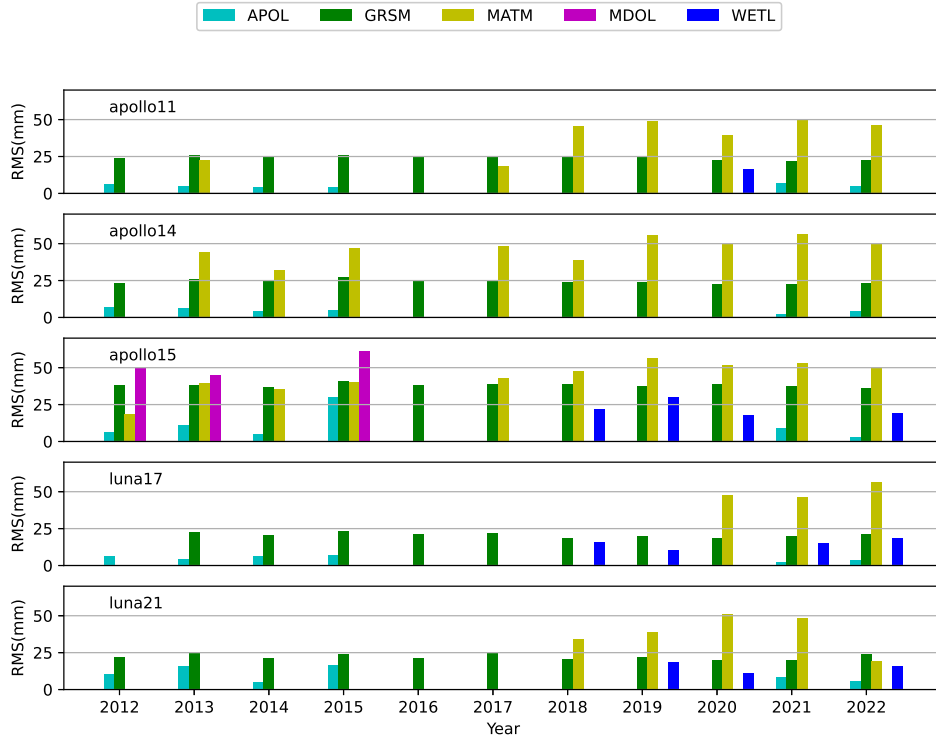
Fig. 3: The lunar laser ranging measurement uncertainty in the form of NP RMS, values in millimeters, for five reflector targets, at five stations, during 2012 to 2022. A missing bar means no available data in that station during that year.

Table 3: Common view events during 2012-2022, categorized by station pair and reflectors. The Apollo15 reflector and the GRSM-MATM station pair took most of their category, respectively.

Station pairs	Total NPs	Reflectors				
		Apollo-11	Apollo-14	Apollo-15	Luna-17	Luna-21
GRSM-MATM	126	17	5	91	3	10
GRSM-WETL	55	——	——	25	27	3
APOL-MDOL	3	——	——	3	——	——

$y = \sqrt{0.1x}$ to depict the quantitative relation between them, as shown in Figure 4. The uncertainty trend curve allows for an estimation of the solution error, before comparison with reference values. If the goal is to filter out errors exceeding 1.5 arc seconds, we filter those precision values exceeding 22.5 arc seconds instead.

Out of 184 solutions, we filtered out 9.2% or 17 common view solutions with solution precision larger than 22.5 arc seconds. The remaining 90.8% or 167 solutions yielded for x_p a mean of -54 mas, with a standard error of 394 mas or RMS of 398 mas, and for y_p a mean of -14 mas, with a standard error of 392 mas or RMS of 392 mas . There were 29.3% or 54 solutions inside the circle with a 150 mas radius,

as shown in Figure 6(b). There were 21.7% or 40 solutions that exhibited less error than the predicted data, i.e., improved over the prediction.

The solutions of GRSM+MATM spreads wider in x_p component, while the solutions of GRSM+WETL spreads wider in y_p component, as shown in Figure 6(a).
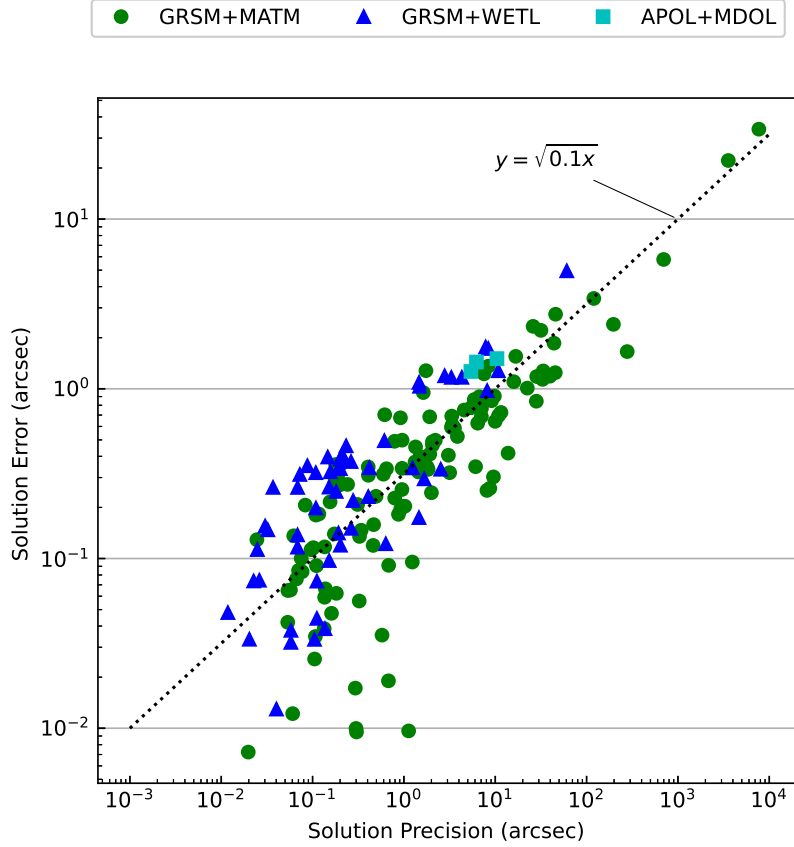

Fig. 4: The correlation of solution error versus solution precision, in log-log scale. All 184 solutions are shown in this figure. The error data presented is the square root of the sum of the squared PMC errors. The solution precision data is calculated as mentioned in subsection 2.3. The curve $y = \sqrt{0.1x}$ serves as an empirical trend that aligns closely with the observed correlation.

5 DISCUSSION AND CONCLUSION

The paper established the method to solve Earth's PMC with instant LLRCV measurements. We compared the solution with the IERS EOP 20 C04 time series. The x_p and y_p solution errors had mean of -54 mas and -14 mas, with RMS errors of 398 mas and 392 mas, respectively. There is no similar result in the literature, but if we compared our results with the best results of the mainstream method (WRMS values of 1.30 mas and 1.63 mas) (Singh et al. 2022), the error is about 300 and 240 times larger, respectively . There were 21.7% of cases outperformed the prediction of the linear polar motion model. Overall, this result indicates that the instant determination of polar motion coordinates is possible.

There are unsolved problems in this approach. The quality of solution differs between station pairs. Systematic trends exist in the solutions of both European station pairs as shown in Figure 6(a). It may be
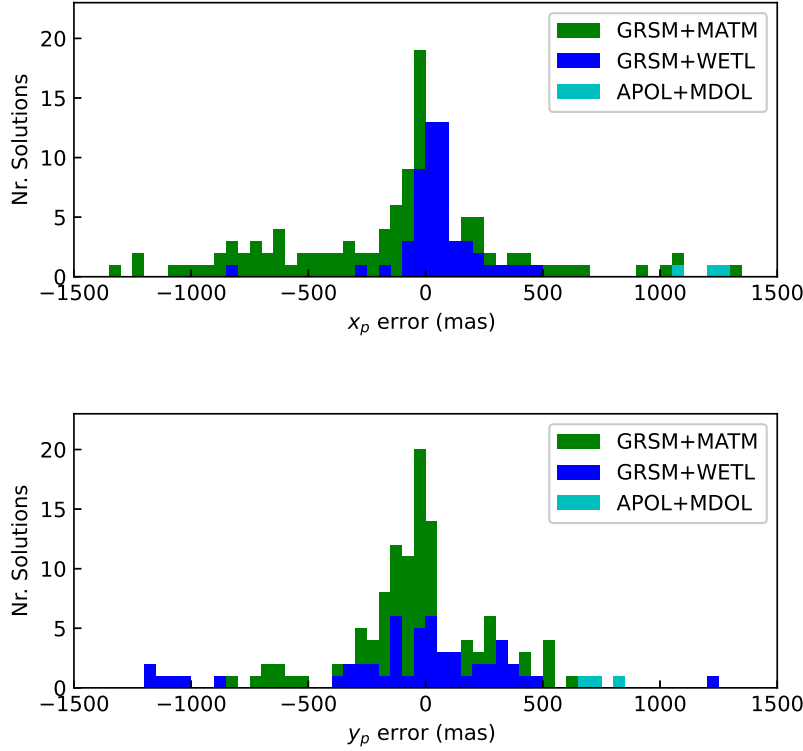
Fig. 5: Solution error distribution of polar motion components. The errors were generated in comparison with the IERS C04 EOP dataset. There are 92.9% (171 of 184) solutions shown in this figure. The GRSM+MATM solutions (green) concentrated around zero, in both x_p and y_p components. The GRSM+WETL solutions (blue) concentrated around zero in the x_p component, but spread in the y_p component.

the near distance between members of a station pair that can affect the precision of the solution. For the GRSM+MATM pair, station coordinate error may be a significant error source, since the MATM part of range residuals had decimeter level bias in this paper, as shown in Figure 2(a). The quality of solution could be improved using a better LLR model, more precise station coordinates, and more precise PMC predictions.

The rapid solution has the potential to address short-term and transient geophysical changes. However, the method relies on long-term geodetic products, therefore, it cannot replace conventional solutions.

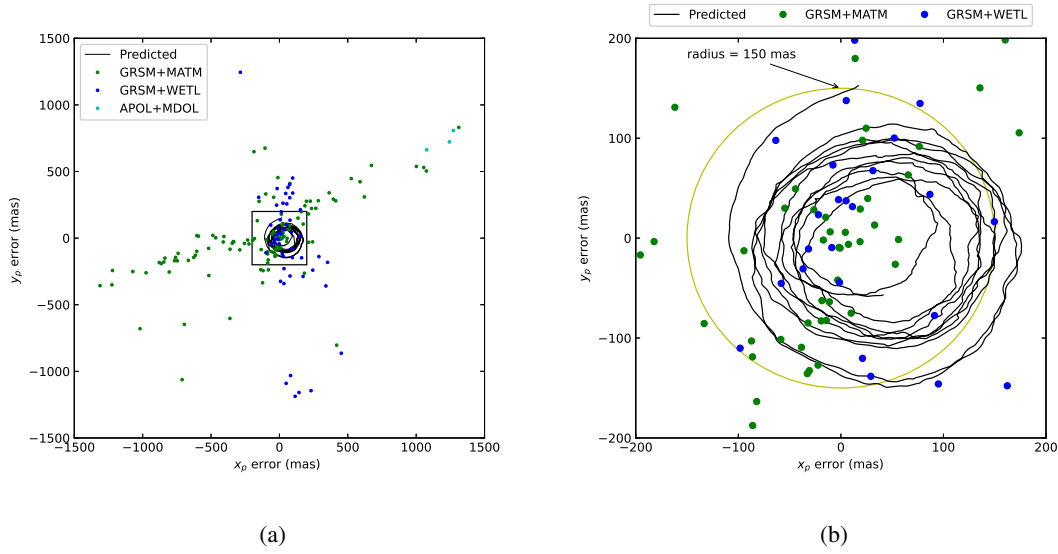(a)   (b)

Fig. 6: Polar motion solution error in two dimensions. In (a), a large map spans ±1500 mas in both x_p and y_p axes, containing 92.9% (171 of 184) solutions. The GRSM+MATM (green dots), GRSM+WETL (blue dots), and APOL+MDOL (cyan dots) represent their deviation from reference data of the corresponding common view solutions. The Predicted (grey curve) near the origin represents a polar motion prediction error. Trends can be seen from lower left to upper right (green) and from up to down (blue). The central box marks ±200 mas for both the x_p and y_p coordinates. In (b), the same map is enlarged to show the area enclosed by the central box in (a). The span in x_p and y_p axes are both ±200 mas, containing 37.5% (69 of 184) solutions. The predicted (grey curve) represents polar motion prediction error. The GRSM+MATM data (green dots) and GRSM+WETL data (blue dots) represent their deviation from reference data of the corresponding common view solutions. A central circle (yellow) with a radius of 150 mas is shown for comparison. There are 29.3% or (54 of 184) solutions in the circle.

References

Altamimi, Z., Rebischung, P., Collilieux, X., Metivier, L., & Chanard, K. 2023, Journal of Geodesy, 97 6

Bender, P. L., Currie, D. G., Dicke, R. H., et al. 1973, Science, 182, 229 2

Chabé, J., Courde, C., Torre, J.-M., et al. 2019, Earth and Space Science, 7 2

Chapront, J., & Francou, G. 2006, Lunar Laser Ranging: measurements, analysis, and contribution to the reference systems, ed. J. S. (eds.) & M. Feissel-Vernier, Vol. 34, IERS Technical Note No. 34 The International Celestial Reference System and Frame, ed. J. S. (eds.) & M. Feissel-Vernier, Vol. 34 (Frankfurt am Main: Verlag des Bundesamts f¨ur Kartographie und Geod¨asie), 97 3

Dickey, J. O., Newhall, X. X., & Williams, J. G. 1985, Journal of Geophysical Research-Solid Earth and Planets, 90, 9353 3

Folkner, W. M., Williams, J. G., Boggs, D. H., Park, R. S., & Kuchynka, P. 2014, Interplanetary Network Progress Report, 42-196, 1 4

Hofmann, F., Biskupek, L., & Müller, J. 2018, Journal of Geodesy, 92, 975 2, 3, 6

Hohenkerk, C. 2012, Proceedings of the International Astronomical Union, 10, 225 4, 12

Huang, K., Sun, S.-B., Yang, Y.-Z., et al. 2022, Laser & Optoelectronics Progress, 197 2

Ji, J. H., Tan, D. J., Bao, C. H., et al. 2023, Research in Astronomy and Astrophysics, 23 4, 12

Leick, A. 1980, Bulletin Géodésique, 54, 55 2, 3

Luzum, B., & Petit, G. 2012, Proceedings of the International Astronomical Union, 10, 227 4

Luzum, B., Thaller, D., Lemoie, F., et al. 2020, Journal of Geodesy, 94, 293 6

Murphy, T. W. 2013, Reports on Progress in Physics, 76, 076901 2, 3

Müller, J., Biskupek, L., Oberst, J., & Schreiber, U. 2009, Contribution of Lunar Laser Ranging to Realise Geodetic Reference Systems, ed. H. Drewes, Geodetic Reference Frames: IAG Symposium Munich, Germany, 9-14 October 2006, ed. H. Drewes (Berlin, Heidelberg: Springer Berlin Heidelberg), 55 2, 3

Müller, J., Murphy, T. W., Schreiber, U., et al. 2019, Journal of Geodesy, 93, 2195 2, 3

Pavlov, D. 2020, Journal of Geodesy, 94 2, 3

Pearlman, M. R., Noll, C. E., Pavlis, E. C., et al. 2019, Journal of Geodesy, 93, 2161 11

Petit, Gérard; Luzum, B. 2010, IERS Conventions (2010), IERS Technical Note (Frankfurt am Main: Verlag des Bundesamts für Kartographie und Geodäsie), 179 4, 5, 6, 12

Price-Whelan, A. M., Lim, P. L., Earl, N., et al. 2022, Astrophysical Journal, 935 4, 12

Samain, E., Mangin, J. F., Veillet, C., et al. 1998, Astronomy and Astrophysics Supplement Series, 130, 235 2

Shores, T. S. 2018, Applied Linear Algebra and Matrix Analysis, 2nd edn., Undergraduate Texts in Mathematics (Springer Cham) 5

Singh, V. V., Biskupek, L., Müller, J., & Zhang, M. Y. 2022, Advances in Space Research, 70, 2383 2, 10

Stolz, A., Bender, P. L., Faller, J. E., et al. 1976, Science, 193, 997 2

Williams, J. G., Boggs, D. H., & Folkner, W. M. 2013, DE430 Lunar Orbit, Physical Librations, and Surface Coordinates, Report IOM 335-JW,DB,WF-20130722-016, JET PROPULSION LABORATORY, CALIFORNIA INSTITUTE OF TECHNOLOGY 4

Xu, C., & Sun, W. 2012, Geodesy and Geodynamics, 3, 28 2

Xu, C., Sun, W., & Chao, B. F. 2014, Journal of Geophysical Research: Solid Earth, 119, 9031 2

Yan, Y.-S., & Guo, J.-F. 2024, Journal of Astronautics, 661 2